Physica C: Superconductivity and its applications 529 (2016) 1–7

Contents lists available at ScienceDirect

Physica C: Superconductivity and its applications

journal homepage: www.elsevier.com/locate/physc

Giant flux jumps through a thin superconducting nb film in a vortex free region

M.I. Tsindlekht[a,*], V.M. Genkin[a], I. Felner[a], F. Zeides[a], N. Katz[a], Š. Gazi[b], Š. Chromik[b]

[a] The Racah Institute of Physics, The Hebrew University of Jerusalem, Jerusalem 91904, Israel
[b] The Institute of Electrical Engineering SAS, Dúbravská cesta 9, 84104 Bratislava, Slovakia

ARTICLE INFO

Article history:
Received 1 May 2016
Revised 4 August 2016
Accepted 8 August 2016
Available online 9 August 2016

PACS:
74.25.F-
74.25.Op
74.70.Ad

Keywords:
Superconductivity
Thin-walled cylinders
Flux jumps

ABSTRACT

We measure the dynamics of magnetic field penetration into thin-walled superconducting niobium cylinders. It is shown that magnetic field penetrates through the wall of a cylinder in a series of giant jumps with amplitude 1 - 2 mT and duration of less than a microsecond in a wide range of magnetic fields, including the vortex free region. Surprisingly, the jumps take place when the total current in the wall, not the current density, exceeds a critical value. In addition, there are small jumps and/or smooth penetration, but their contribution reaches only $\simeq$ 20 % of the total penetrating flux. The number of jumps decreases with increased temperature. Thermomagnetic instabilities cannot explain the experimental observations.

1. Introduction

The study of magnetic flux penetration into superconductors has a longstanding scientific tradition. The physics of this phenomenon in type II superconductors, for the magnetic field parallel to the sample surface, is seemingly straightforward. For magnetic fields below H_{c1} (in the Meissner state) the fields are totally expelled from the sample. Whereas above H_{c1} the flux penetrates via Abrikosov vortices. However in real superconductors, due to defects the vortex distribution is not uniform and in this case the vortex lattice is in a metastable state. The metastable states of the vortices are the cause of numerous physical phenomena such as: flux creep, magnetic relaxation [1,2] and vortex avalanches, see review by Altshuler and Johansen and references therein [3]. The explanation of vortex avalanches was given mainly in the framework of two models: thermomagnetic instabilities [4] and self-organized criticality (SOC) [5]. Bean's critical state [6] is the basis for both models. This model is valid when the dimensions of the sample are much larger than London's penetration depth, λ, and correlation length, ξ. In the case of a thin planar film it takes place in magnetic fields perpendicular to film surface. The avalanche-like penetration of magnetic flux into a type II superconductor was studied by numerous experimental methods. The most popular methods are magneto-optical imaging, micro-Hall-probe and pick-up coil experiments [3]. Subsequently in this paper we will focus mainly on experiments with a pick-up coil. In the long tradition of pickup coil experiments [7,8] voltage spikes that were induced in the pick-up coil by the magnetic moment jumps caused by a swept field were measured. Magnetic moment jumps at high field sweep rate, up to 0.1 T/s, were accompanied by increasing the sample temperature due to rapid motion of the vortex bundles [7,8]. Thermomagnetic instabilities are the cause of such heating [4]. However, at low sweep rates, the heating produced by a flux jump did not play a significant role [9,10]. The experimentally observed avalanche size distribution, which indicates the number of vortices in a moving bundle, is an exponential [9] or a power-law [10] function of the avalanche size. The latter experimental fact was used as a confirmation of SOC model [10]. It was demonstrated that the magnetic flux penetrates into the interior of the cylinder in two fashions. The first one is a smooth flux flow and the second one is jump like. The contribution of the smooth flow for a thick-walled cylinder was about 97% of the total penetrated flux [10]. Experiments reported in [10,11] were performed on hollow cylinders with large wall thickness $d \gg \lambda$. In this case, as expected, avalanches were detected in magnetic fields higher than H_{c1}, i.e. in a mixed state. Concurrently, we have shown that for a thin-walled cylinders of Nb, $d \leq \lambda$, an "avalanche"-like magnetic flux penetration occurs not only in magnetic fields higher but in

* Corresponding author. Fax.: +972 26586347.
E-mail address: mtsindl@vms.huji.ac.il (M.I. Tsindlekht).

http://dx.doi.org/10.1016/j.physc.2016.08.005
0921-4534/

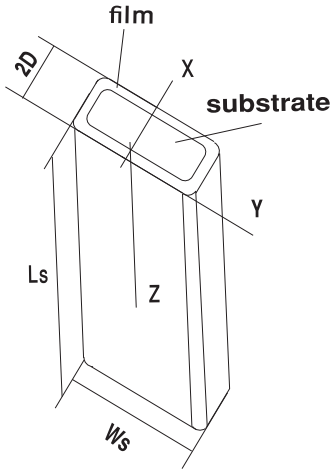

Fig. 1. Sketch of the rectangular sample. Here $W_s = 3$ mm, and $2D = 1.4$ mm are the substrate width and thickness, respectively, with variable length, L_s.

Table 1
Labels and properties of the samples discussed in the text .

Sample label	d (nm)	Cross-section shape	Length (mm)	Deposition temp. (°C)
F1	60	rectangular	15	300
F8	120	rectangular	15	300
F15	300	rectangular	15	300
G7	100	rectangular	7.5	20
G21	100	rectangular	21	20
G3a	100	circular	7.5	20

lower than H_{c1} of the film itself, i.e. in the vortex free region [12]. The latter phenomenon is very interesting, and the physical reasons for it are not yet clear.

In this paper, we present a comprehensive experimental study of the dynamics of magnetic flux penetration into thin-walled superconducting Nb cylinders. The magnetic field penetrates through the walls of the cylinder in a series of giant jumps with magnetic field amplitude 1 - 2 mT and duration of less than a microsecond (exact timing cannot be resolved by our setup). The jumps take place when the total current in the wall, not the current density, exceeds some critical value. The giant jumps were observed in fields below and above H_{c1} of the Nb film itself. In addition to the avalanche-like penetration there is a smooth penetration and its contribution can reach about 20% of the total penetrated flux. This is in stark contrast with the previous experiments which were dominated by such a smooth penetration of flux [10]

2. Experimental details

2.1. Samples and block diagram of experimental setup

Various thin-walled cylindrical samples with two cross-section shapes were prepared by dc magnetron sputtering of Nb on a rotated sapphire and glass substrates at room temperature (Bratislava) and at 300° C (Jerusalem). Sapphire substrates were manufactured by Gavish Ltd company (Israel). The cross-section dimensions of the long parallelepiped sapphire substrates were 1.4 by 3 mm. The corners of these substrates were rounded to a radius of 0.3 mm. A sketch of the rectangular sample is shown in Fig. 1. The glass substrate has a circular cross-section with a diameter of 3 mm. The lengths, film thicknesses, deposition temperatures and labels of the samples are presented in the Table 1.

The samples were inserted into a multi-layer pick-up copper coil of 14 layers, length L = 15 mm and total number of the turns

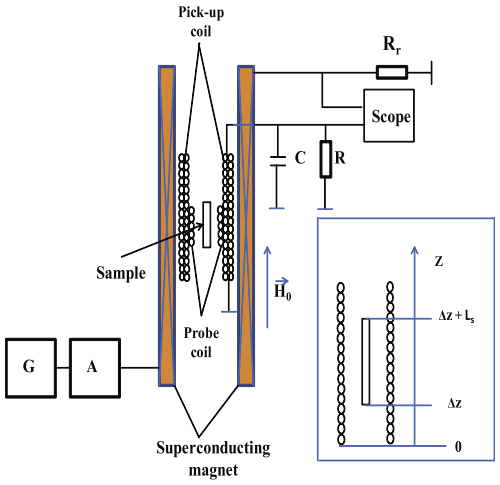

Fig. 2. (Color online) Block diagram of the experimental setup. Here **C** is a capacitor of the coaxial cables, **R** is a shunt resistor for damping oscillations in a resonant circuit, **G** is 33250A Agilent generator, **A** is amplifier, and $\mathbf{R_r}$ is a current sensing resistor. Superconducting magnet is a part of the SQUID magnetometer. Inset: Layout of the pick-up coil, sample and the orientation of the Z-axis. See text.

N = 2100 turns, which was placed in a commercial superconducting quantum interference device (SQUID) magnetometer, MPMS5, Quantum Design. External magnetic field, H_0, was directed parallel to the long axis of the sample and pick-up coil. The superconducting magnet of the SQUID magnetometer was driven by an arbitrary waveform generator, Agilent 33250A, and a home-built amplifier. The applied field was slowly changed with a rate of: 0.4, 0.8, or 1.6 mT/s from zero to 0.186 T and then back to zero. The voltage spikes induced by a swept magnetic field were measured by an InfiniiVision, DSO-X 3024A, Agilent oscilloscope with bandwidth 200 MHz. Time resolution of the whole system is order of 0.1 μs An additional channel of the oscilloscope was used for magnetic field measurement. Fig. 2 shows a block diagram of the experimental setup.

2.2. Pick-up coil calibration

To calibrate the pick-up coil we wound a small probe coil with $n_p = 30$ turns and radius $a_p = 2$ mm under the pick-up coil and drove it by a current jump. A magnetic flux Φ_1 induced in one turn of the pick-up coil by a linear circular current J with radius a is [13]

$$\Phi_1 = \frac{\mu_0 J}{4\pi}\int_0^{\pi}\frac{a r_l \cos(\varphi)d\varphi}{(a^2 + r_l^2 + \tilde{z}^2 - 2a r_l\cos(\varphi))^{1/2}}, \quad (1)$$

where $\tilde{z}$ is the distance between these two circles which are parallel to each other, μ_0 is permeability of vacuum and r_l is radius of the turn in l^{th} layer of the pick-up coil. From this expression we get the magnetic flux through the one layer of pick-up coil

$$\phi = \frac{\mu_0 a^2 J n}{4\pi L}\Phi_q(r_l/a, z/a, L/a), \quad (2)$$

where

$$\Phi_q(r,z,l) = r\int_0^{\pi} d\varphi\cos(\varphi)\ln \times\left(\frac{(1+r^2+(l-z)^2-2r\cos(\varphi))^{1/2}+(l-z)}{(1+r^2+z^2-2r\cos(\varphi))^{1/2}-z}\right) \quad (3)$$

is a dimensionless function, z is the Z-coordinate of the circular current and n is a number of turns in one layer of the pick-up coil ($n \approx 150$). The coordinates of the pick-up coil ends are 0 and L, see inset in Fig. 2. Fig. 3 shows $\Phi_q(z)$ for two values of radius a, 1.16

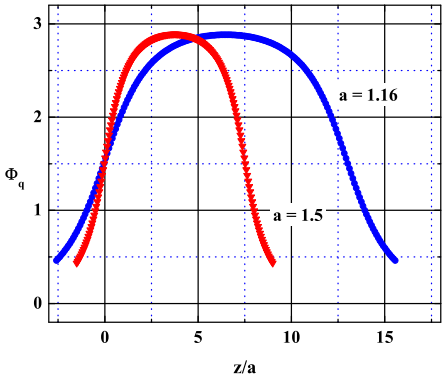

Fig. 3. (Color online) Φ_q versus z.

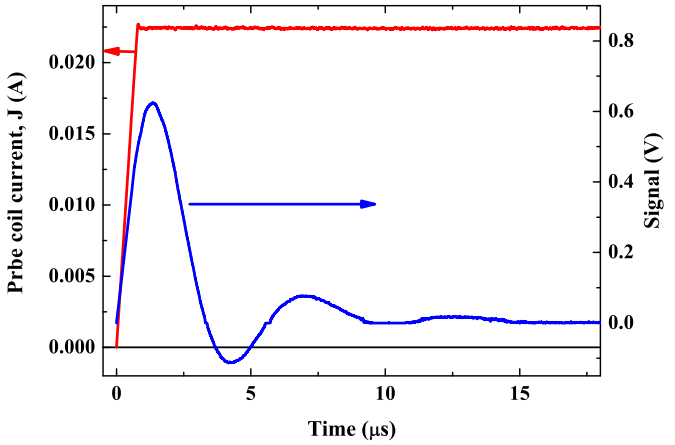

Fig. 4. (Color online) Current in the probe coil and the voltage on the pick-up coil as a function of time.

and 1.5. For n_p turns of the probe coil of radius a_p and length $l_p \ll L$, located in a center of the pick-up coil, $z_0 = L/2$, we obtain

$$\phi = \mu_0 n_p \frac{a_p^2 Jn}{4\pi L} \Phi_q(r_l/a_p, L/2a_p, L/a_p). \tag{4}$$

Now we assume that a thin-walled circular hollow tube with length L_s, radius a_t, and wall thickness $d \ll a_t$ is inserted symmetrically into the pick-up coil and ΔH is the difference between magnetic fields inside and outside the tube. In this case the surface current density in the wall is $j = \Delta H$. Flux that this current creates in one layer of the pick-up coil is

$$\begin{aligned}\phi_l &= \frac{\mu_0 \Delta H}{4\pi} \frac{a_t^2 n}{L} a_t \int_{\Delta z}^{\Delta z + L_s} dz/a_t \Phi_q(r_l/a_t, z/a_t, L/a_t) \\ &= \frac{\mu_0 \Delta H}{4\pi} \frac{a_t^3 n}{L} \Phi_{tl},\end{aligned} \tag{5}$$

where Δz is a distance between the edges of the tube and pick-up coil. The Φ_{tl} can be calculated by a numerical integration of the data presented in Fig. 3. Equation (5) for a circular tube is applied for a rectangular tube with the same cross section area.

Measured by scope signal is a linear function of the emf in the pick-up coil. This has been checked experimentally. The response of a linear system is linear with the input signal. As for any linear system the measured by scope signal $V(t)$ due to the change the magnetic flux through the all pick-up coil layers, $\phi_f = \sum_l \phi_l$, is

$$V(t) = \int_0^t d\tau K(t-\tau) \frac{d\phi_f(\tau)}{d\tau}, \tag{6}$$

where $K(t)$ is the response to the δ-like flux jump. The integral

$$\overline{Q} = \int_0^\infty V(t)dt = \Delta\phi_f \int_0^\infty K(t)dt \tag{7}$$

is proportional to the total change of magnetic flux in the pick-up coil.

The change of magnetic field inside a tube can be found from the time dependant voltage in the pick-up coil and the response to the current jump in the probe coil from

$$\mu_0 \Delta H = n_p J \sum_l \left(\frac{a_p^2}{a_t^3} \frac{\Phi_q(r_l/a_p, L/2a_p, L/a_p)}{\Phi_{tl}} \right) \frac{\overline{Q}_s}{\overline{Q}_p} = 10^{-4} D \frac{\overline{Q}_s}{\overline{Q}_p}, \tag{8}$$

where $\overline{Q}_{p,s} = \int_0^\infty V_{p,s}(t)dt$ which were calculated for $V(t)$ obtained in experiments with the probe coil and sample. Parameter D in Eq. (8) was calculated and it is approximately equal 2.2 for samples F1, F8, F15 and G3a, 1.8 and 3.7 for samples G21 and G7, respectively. In calculations of this parameter we took into account that the radius of the first layer of the pick-up coil is 2 mm and the last one 4 mm. Fig. 4 shows a signal in the pick-up coil in response to the current jump in the probe coil. We have to note that integral $\int_0^\infty K(t)dt$ drops out of the formula (8).

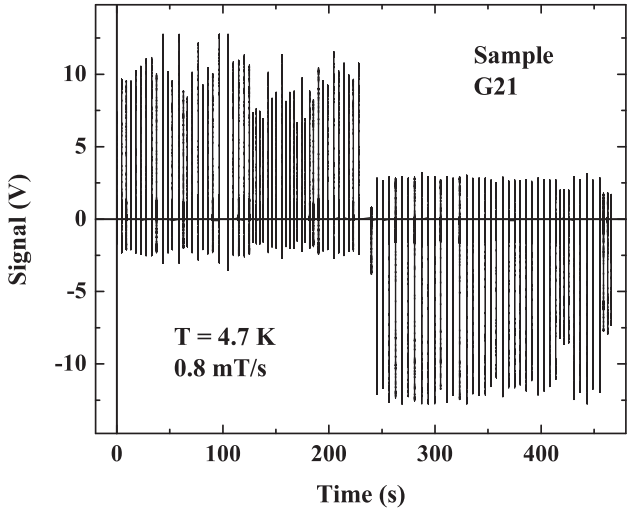

Fig. 5. Sequence of pulses in sample G21 at T = 4.7 K and seep rate 0.8 mT/s.

3. Experimental results

Fig. 5 presents the voltage pulse sequence for sample G21 at 4.7 K. The sample was zero field cooled (ZFC). Then the field was slowly ramped with a rate of 0.8 mT/s to 0.186 T and then swept back to zero. Each vertical line in Fig. 5 is actually the time dependent voltage signal as shown in Fig. 6. The signal changes its polarity when the magnetic field starts to decrease. Increasing the rate to 1.6 mT/s did not cause any considerable change. Note that slowly ramping magnetic field induces a small voltage on a pick-up coil due to smooth flux or small jumps' penetration. This small voltage cannot be detected by our setup. The magnetic field H_n at which n^{th} jump takes place and total number of jumps varies from run to run. Fig. 7 demonstrates few subsequent measurements of H_n at 4.7 K for F8 sample after ZFC at each run.

The total number of jumps dramatically decreases with temperature and they completely disappear near 5.6 K, as shown in Fig. 8 panel *a*. The temperature dependences of ΔH_n (Eq. (8)) and H_n for the first three jumps of sample F8 are presented in Fig. 8 panels *b* and *c*, respectively. The first jump at 4.7 K occurs in field $\mu_0 H_1 \approx 2.1$ mT (Fig. 8(c)) and at this jump $\mu_0 \Delta H_1 \approx 2.1$ mT, Fig. 8(b). Thus, after the first jump the field inside the cylinder equals the external one. Estimation of the relative role of large jumps on the flux penetration can be obtained from data shown in Fig. 9. This figure shows the calculated field inside a

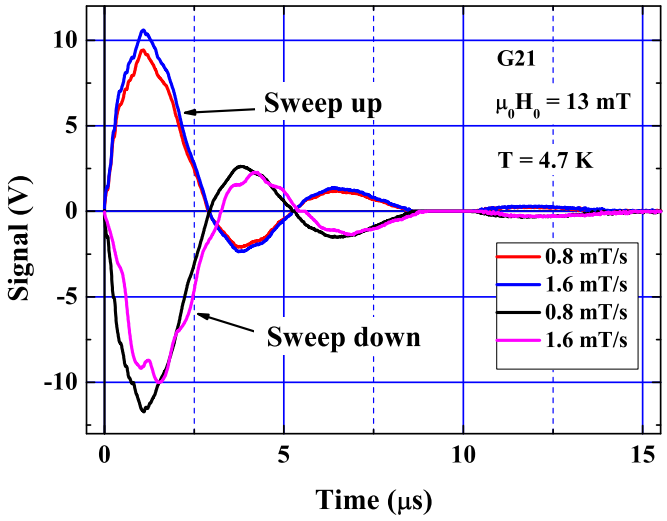

Fig. 6. Signals at $\mu_0 H_0 = 13$ mT in ascending and descending fields that was observed in sample G21.

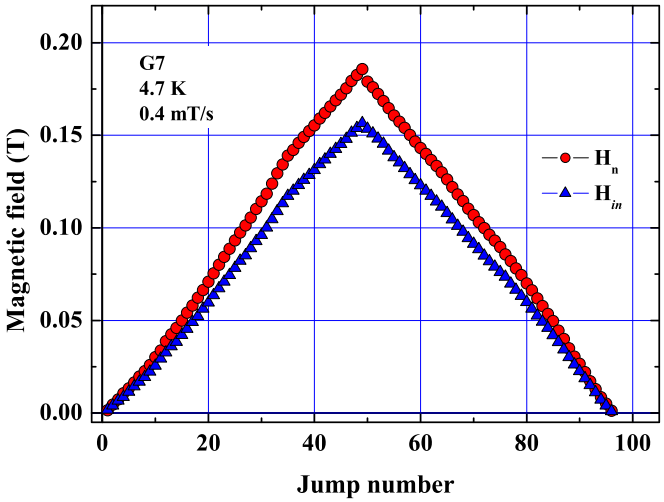

Fig. 9. (Color online) H_n and H_{in} as a function of jump number for sample G7.

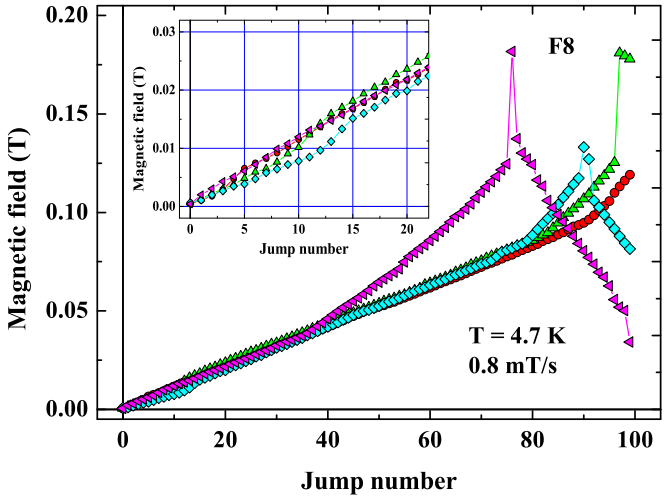

Fig. 7. (Color online) Magnetic field at which the jump was observed, H_n, as a function of jump number. Subsequent measurements were repeated and done after ZFC. Inset shows an expanded view of these curves at low magnetic fields.

cylinder after n jumps, $H_{in} = \sum_{i=1}^{n} \Delta H_i$, for sample G7 as a function of the jump number assuming that all penetrations are via large jumps only. The maximal value after 49 jumps of $\mu_0 H_{in}$ for sample G7 is $\approx$ 0.157 T - average value of $\mu_0 \Delta H$ per one jump is about 3.2 mT. The average magnetization of sample G7 at $\mu_0 H_0 \approx 0.186$ T is $\mu_0 m \approx -3$ mT. The magnetic induction inside the cylinder $B = \mu_0 (H_0 + m) \approx 0.183$ T, and the average $\mu_0 \Delta H$ per one jump is ≈ 3.7 mT. It means that only ≈ 0.5 mT per jump penetrate through the wall via small jumps and/or smooth flux penetration. These data show that the field penetrates through the walls via large jumps and the contribution of other undetected small jumps and/or smooth penetration are small. This is in contrast with reported 97% contribution for fields above H_{c1} in a thick-walled cylinder [10].

Fig. 10 (a) depicts H_n as function of the jump number n for samples F1 and F15 with wall thickness 60 and 300 nm, respectively. The jumps for sample F1 disappear when the applied field exceeds 0.11 T, whereas for sample F15 the last jump was observed around 0.15 T. The average difference between H_n of neighboring $\mu_0 dH_{av} = \mu_0 \langle H_n - H_{n-1} \rangle$ in ascending field equals $\approx$ 1.7 and $\approx$ 2.5 mT for samples F1 and F15, respectively. For the first 20 jumps at low fields, $\mu_0 H_0 \leq 32.0$ mT, the $\mu_0 dH_{av}$ decreases to $\approx$ 1.4 and 1.6 mT for samples F1 and F15, respectively. The inset to Fig. 10(a) shows an expanding view of H_n versus n at low fields. The magnetic field that penetrates during each jump ΔH_n depends on the change in field from the previous jump, $H_n - H_{n-1}$, as it is shown Fig. 10(b) for samples F1 and F15. Inset to Fig. 10(b) presents ΔH_n as a function of H_n for several first jumps. These data are scattered and the difference between these two sets is not essential regardless of the fivefold difference in the walls thickness.

Fig. 11 (a) shows H_n as a function of n for samples G3a and G7 at 4.7 K with different cross-section shape. The average field distance between adjacent jumps, dH_{av}, is lower for sample G3a

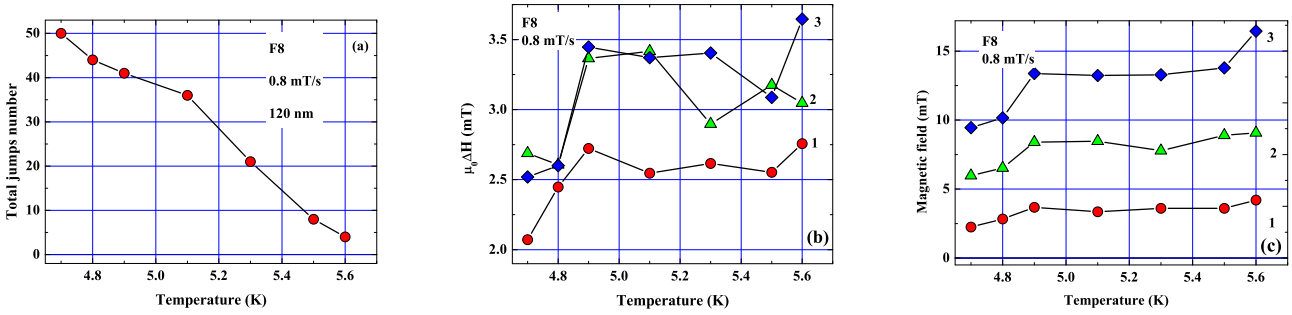

Fig. 8. (Color online) Panel *a*: The total jump number in ascending field versus temperature. Panel *b*: Temperature dependence of the first three field jumps, ΔH_n, see Eq. (8). Panel *c*: Magnetic field of the first three jumps as a function of temperature. The number near the curves in panels *b* and *c* is the jump number. The data presented in all three panels were obtained in an ascending field at a sweep rate of 0.8 mT/s.

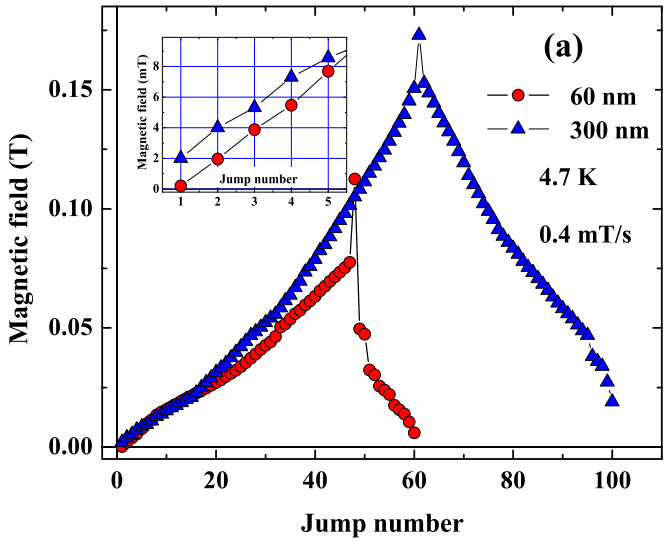

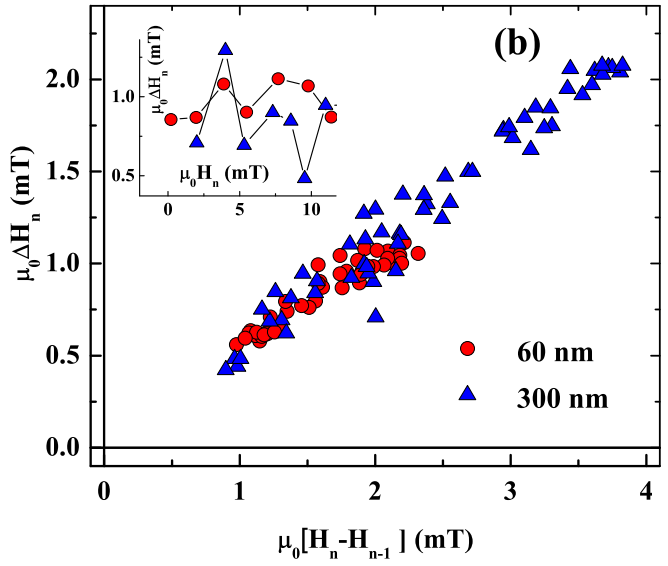

Fig. 10. (Color online) Panel *a*: Magnetic field of jump as a function of jump number for F1 and F15 samples. The first 100 jumps are shown only. Expanded view for the first five jumps is presented in inset. Panel *b:* ΔH_n as a function of $H_n - H_{n-1}$ for F1 and F15 samples. ΔH_n as a function of the magnetic field is shown at the inset to panel *b*.

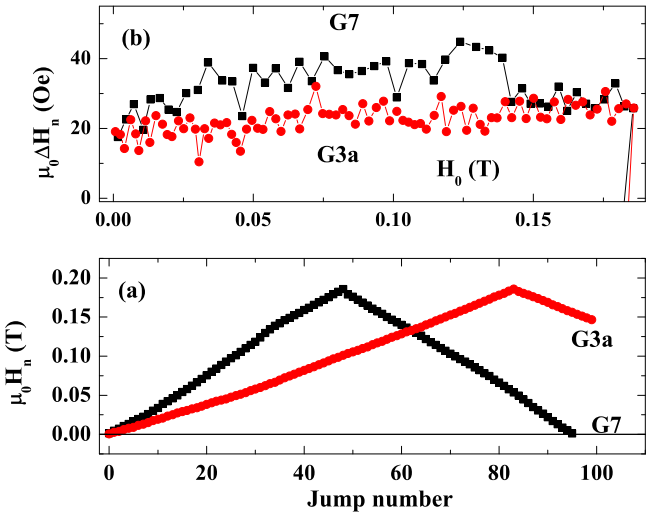

Fig. 11. Panel *a:* H_n as a function of jump number for samples G3a and G7 at 4.7 K. Panel *b*: Field dependence of ΔH_n for samples G3a and G7.

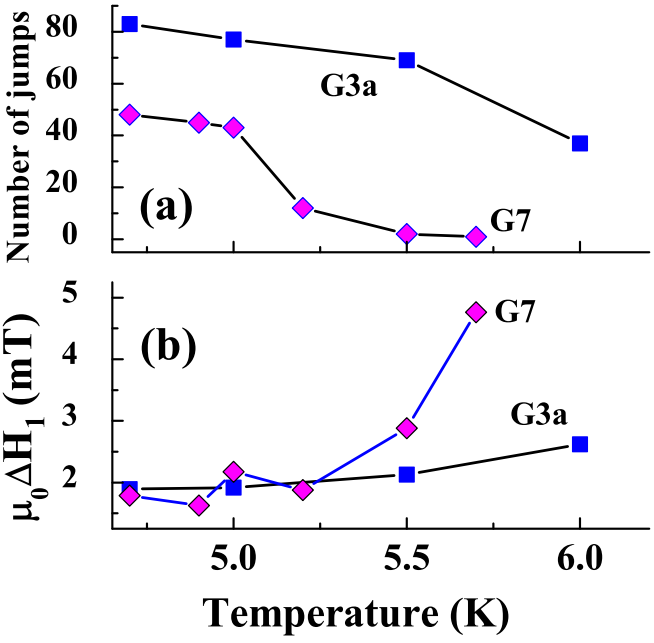

Fig. 12. Panel *a*: The total number of jumps for samples G3a and G7 versus temperature in ascending magnetic field. Panel *b:* ΔH_1 as a function of temperature for G3a and G7 samples.

and then amplitude of the field jump ΔH_n is also lower than for sample G7, Fig. 11b. The total number of jumps in ascending field as a function of temperature for G7 and G3a samples is presented in Fig. 12*a*. Temperature dependences of $\Delta H_1(T)$ for samples G3a and G7 are demonstrated in Fig. 12(*b*). The comparison of these two sets of experimental data shows that there are quantitative differences between samples G3a and G7. The difference of the responses the samples G3a and G7 could be associated with the structure of the films, shape of the substrate and type of the substrates. However, it is evident that qualitatively the data for these two samples are similar because the waveform of the signals for two samples is actually the same and values of H_n, ΔH_n varies from run to run.

4. Discussion

The most striking phenomenon observed here is the magnetic field "avalanche"-like penetration into thin-walled cylinder under external fields below H_{c1}. Estimations the H_{c1} and H_{c2} of the walls were obtained from the magnetization curve of the film which was deposited on planar substrate during the fabrication of a cylindrical sample. Fig. 13 demonstrates ascending branch of the magnetization curve of a planar film in magnetic field parallel to its surface. H_{c1} was defined by the deviation from linearity the magnetization curve at low fields and it is $\approx$ 35.0 mT. Using data for H_{c1} and $\mu_0 H_{c2} \approx 0.9$ T, see Fig. 13, we can estimate λ and ξ. It turns out that $\lambda \approx 120$ nm and $\xi \approx 20$ nm at 4.5 K. Film thickness of our samples varies from 60 to 300 nm. For films with such thicknesses H_{c1} is a weak function of the thickness [15]. Although the method of H_{c1} determination is not accurate, jumps of the magnetic

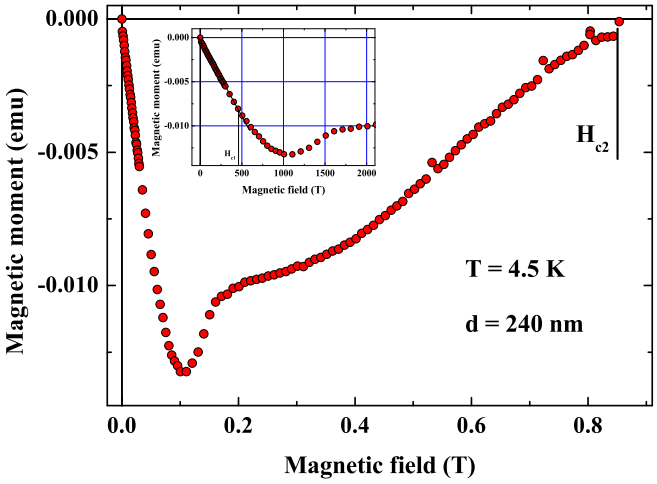

Fig. 13. Magnetization curve of a planar film at 4.5 K. Inset: Expanded view of $M(H_0)$ at low magnetic fields.

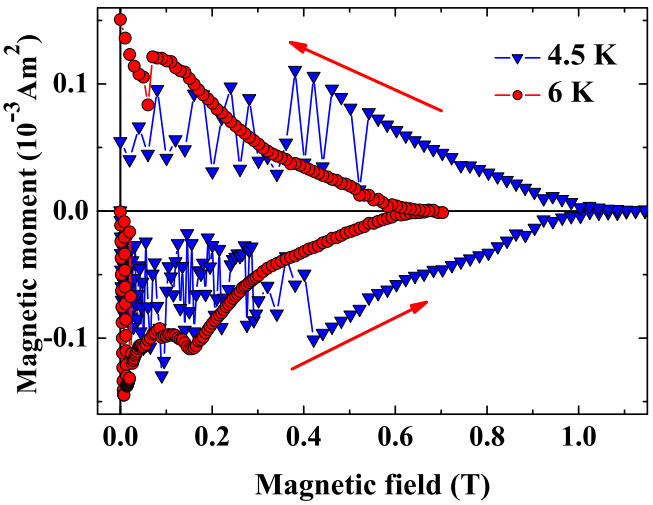

moment into cylindrical samples were observed at fields of 2 - 4 mT, which are significantly lower than $\mu_0 H_{c1}$ regardless of any uncertainty. Fig. 14 shows magnetization curves of the G7 sample at 4.5 and 6 K (upper panel). The lower panel of this figure demonstrates an expanded view of these curves at low magnetic fields. One can see that after the jump the superconducting state is restored see Fig. 14, lower panel. Above a specific jump at low fields the magnetic moment is a linear function of a magnetic field with dM/dH_0 that corresponds to complete screening.

There are two possible superconducting states of a hollow cylinder in a magnetic field parallel to its axis: (i) a metastable state with the internal magnetic field different from the external one and non-zero total current in the wall, and (ii) a stable state with equal magnetic fields and zero total current in the wall. For these two states the maximal current density in the wall is actually the same as follows from the solution of the London equation [14]. This solution for a planar film in a magnetic field parallel to the film surface is presented in Fig. 15. Our experiment shows that the total current, not the current density, in the wall is a main parameter which could determine a jump. If the critical current density defines the jump, one could expect that the second jump will occur immediately after the first jump, because maximal current density on the outer side will be approximately the same as before the jump. However, after the jump field inside the cylinder could reach value of the field outside, the total current will be close to zero. If the total current equals zero the currents on the different surfaces of the film opposite to each other and could block the rise of a new jump right after the previous one. Detailed discussion of this problem is beyond the scope of the present paper.

We consider that the physical reason of these jumps is a singularity of the magnetic field at the end faces of the cylinder. The importance of the end faces in thin-walled superconducting cylinders at high frequencies was already discussed in literature many years ago [16]. The authors of this paper argued that the distortion of the magnetic force lines near the end faces is responsible for the observed absorption peculiarities at high frequences. However, to draw a definite conclusion about the role of the end faces it is necessary to solve the problem of the flux penetration into thin-walled cylinder of finite length. To the best of our knowledge, this problem has not yet been solved.

The jumps disappear with increasing temperature, Fig. 8(a) and Fig. 14, lower panel. This resembles the thermomagnetic instability that is often observed in superconductors [3,4]. The thermomagnetic scenario requires the presence of vortices in the walls.

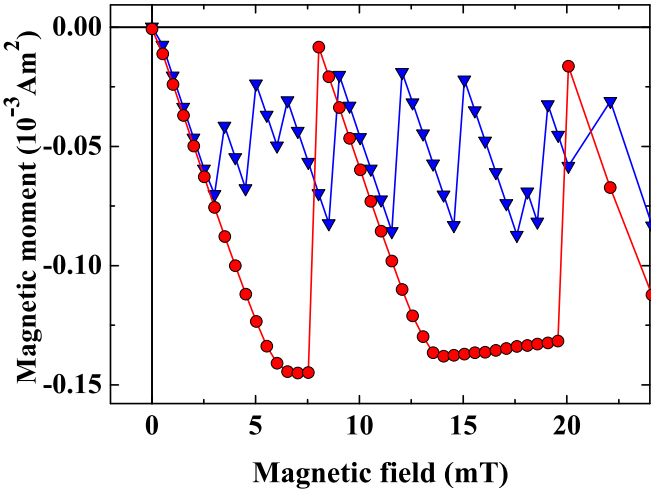

Fig. 14. Upper panel: Magnetization curves of G7 sample at 4.5 and 6 K after ZFC. Lower panel: Expanded view of magnetization curves at low magnetic fields.

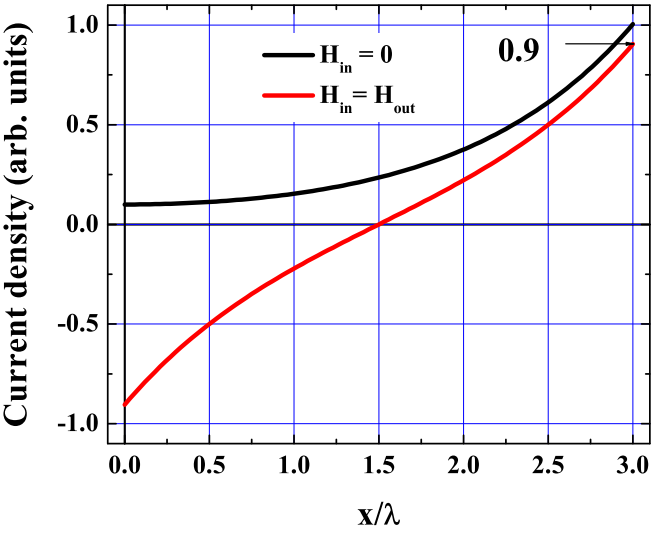

Fig. 15. (Color online) Current density in a film with thickness 3λ as function of coordinate for two cases, first $H_{in} = H_{out}$ - red line and second $H_{in} = 0$ - black line.

In an infinite planar film, in a parallel magnetic field, vortices should only exist at fields larger than H_{c1}. This field is much larger than the fields at which firsts jumps were observed. Together with this our experiment shows that the field of the first jump H_1 increases with temperature whereas below H_1 dM/dH_0 does not depend on the temperature. This is demonstrated for samples F8 and G7 in Figs. 8*c* and 14, respectively. Thermomagnetic instability implies that the critical current decreases with increasing temperature. Here we are faced with the opposite case. At 6 K the first jump takes place for a larger magnetic field, larger total current in the wall, than at 4.5 K. We would like to note that the standard approach to thermomagnetic instability [3,4] is not applicable to the circumstances of our experiment. The theory requires the existence of the Bean critical state in the film [6]. But in a thin film with thickness equal to the size of one or two vortices, the Bean critical state cannot arise.

5. Conclusion

We have studied the dynamics of flux penetration into thin-walled superconducting niobium cylinders. It was shown that magnetic flux penetrates through the walls in a series of giant jumps with duration less than a microsecond. In addition, there is another flux penetration mechanism which contributes $\approx$ 20 % to the total penetrated flux. The current density in the wall does not play an essential role in the observed phenomena. Jumps start when the total current in the wall exceeds some critical value. The jumps were observed at a temperature of 4.5 K and completely disappeared at $\approx$7 K. Such behavior resembles the thermomagnetic instability of vortices but it was observed in fields far below the H_{c1} of the films, i.e. in a vortex-free state. We consider the possibility that the instability at the end faces of the sample could be the cause of these jumps.

Acknowledgments

We thank J. Kolacek, G.I. Leviev, P. Lipavsky and V.A. Tulin for fruitful discussions. We are deeply grateful to Yu. A. Genenko for careful reading of the manuscript and very useful comments. We acknowledge unknown referee for his very useful remarks. This work was done within the framework of the NanoSC-COST Action MP1201. Financial support of the grant agency VEGA in projects nos. 2/0173/13 and 2/0120/14 are kindly appreciated. We acknowledge partial support of ERC grant number 335933.

References

[1] Y.B. Kim, C.F. Hempsted, A. Strnad, Phys. Rev. 131 (1963) 2486.
[2] Y. Yeshurun, A.P. Malozemoff, A. Shaulov, Rev. Mod. Phys. 68 (1996) 911.
[3] E. Altshuler, T.H. Johansen, Rev. Mod. Phys. 76 (2004) 471.
[4] R.G. Mints, A.L. Rakhmanov, Rev. Mod. Phys. 53 (1981) 551.
[5] P. Bak, C. Tang, K. Wiesenfeld, Phys. Rev. Lett. 59 (1987) 381.
[6] C.P. Bean, Phys. Rev. Lett. 8 (1962) 250.
[7] S.H. Goedemoed, C.V. Kolmeschate, J.W. Metselaar, D. De Klerk, Physica 31 (1965) 573.
[8] M.A.R. LeBlanc, F.L. Vernon, J., Physics Lett. 13 (1964) 291.
[9] C. Heiden, G.I. Rochlin, Phys. Rev. Lett. 21 (1968) 691.
[10] S. Field, J. Witt, F. Nori, X. Ling, Phys. Rev. Lett. 74 (1995) 1206.
[11] C.R. Wischmeyer, Phys. Lett. 18 (1965) 100.
[12] M.I. Tsindlekht, V.M. Genkin, I. Felner, F. Zeides, N. Katz, S. Gazi, S. Chromik, Phys. Rev. B 90 (2014) 014514.
[13] L.D. Landau, E.M. Lifshits, Electrodynamics of Continuous Media, Pergamon Press, Oxford, New York, Beijing, Frankfurt, 1984, p. p.112.
[14] P.G. de Gennes, Superconductivity of metals and alloys, W.A. Benjamin, INC, New York, 1966, p. p.197.
[15] A.A. Abrikosov, Fundamentals of the Theory of Metals, North Holland, 1988.
[16] V.M. Zakosarenko, E.V. Il'ichev, V.A. Tulin, Pis'ma v JTF (JTP Lett.) 15 (1989) 41. (in Russian).